Electric Propulsion System Optimization Using Performance Maps

Hong-Su Nam, Hyeon-Su Hwang, Seok-Hwan Lee, and Hak-Tae Lee
Department of Aerospace Engineering
Inha University
Incheon, Republic of Korea 21999
namhs501@inha.edu, 12171214@inha.edu, seokhwan-lee@inha.edu, haktae.lee@inha.ac.kr

***Abstract*— This paper presents a performance map based approach that enables the holistic analysis and design of electric propulsion systems composed of an electronic speed control, a motor, a propeller, and an airframe. As all the performance parameters, including the flight speeds and climb rates, are expressed as contours, this approach provides insights into the performance of the combined propulsion system, not only for a single cruise condition, but for a wide range of operating conditions. First, by using the rotational speed and torque as the two independent variables, the process of computing the efficiency and plotting the efficiency contours for each component is presented. Selected practical techniques, which utilize data provided by the manufacturer, and which do not require costly measurements, are introduced. The approach based on the performance map is applied to evaluate eight combinations of the electronic speed control, motor, and propeller for a two-meter wingspan unmanned aircraft. The results suggest that the maximum range can vary by more than 10% depending on the selection of the components. The methodology described in this paper can be applied to design optimization, component selection for existing airframe as well as mission design and optimization of electric powered aircraft.**

TABLE OF CONTENTS

1. INTRODUCTION

The propulsion system of an electric aircraft has the following basic components: an airframe, a propeller, an electric motor, electronic speed control (ESC), and a battery. Previously, electric propulsion systems were widely used to power small unmanned aircraft. However, in recent years, many companies have started developing electric powered manned aircraft [1]. Optimization of the propulsion system is becoming increasingly important because mismatched components could significantly reduce the overall efficiency of the system resulting in smaller range and endurance for the larger aircraft.

The efficiency of each component under various operating conditions has been extensively studied. Gong and Verstraete [2] tested commercial-off-the-shelf ESCs and presented a curve fit model of the ESC efficiency as a function of the input voltage and current. Larminie and Lowry [3] presented a model for calculating the efficiency of motors by considering power losses such as copper loss, iron loss, friction loss, and windage loss. McDonald [4] presented a positive polynomial loss model of a motor by fitting the measurement data with a non-negative least-squares method. However, little research on establishing an intuitive method, which integrates all the components to verify the total system efficiency, has been reported to date.

McDonald [5] introduced a method for plotting motor efficiency maps and propeller envelopes together on a plane represented by the rotational speed and torque, but did not use detailed propeller efficiency contours. Gong *et al.* [6] presented a method for testing the performance of an electric powered aircraft and introduced the forward flight speed contours on the rotational speed and torque plane. Duan *et al.* [7] used various models of the motor and propeller to optimize the design using particle swarm optimization.

Lee [8] integrated the characteristics of the motor, propeller, and airframe by plotting multiple contours of the component efficiencies as well as other performance parameters on the rotational speed and torque plane. This was one of the first studies that provided a holistic view of an electric propulsion system for a wide range of operating conditions.

The current work is a continuation of [8] with the addition of the ESC efficiency model based on [4] and a higher fidelity propeller efficiency model that reflects the Reynolds number effects. A realistic use case, in which eight different combinations of the ESC, motor, and propeller are compared, is presented. These analyses demonstrated that the range can vary by more than 10% among the combinations of similar components.

Following this introduction, Section 2 describes the power flow of an electric propulsion system as well as how to compute the efficiency of each component from the rotational speed and torque. Section 3 presents the results of evaluating eight different combinations of components to find the one with the maximum range. Finally, Section 4 concludes the paper.

2. ELECTRIC PROPULSION COMPONENTS

A typical electric propulsion system consists of a battery, an ESC, a motor, a propeller, and an airframe. Figure 1 depicts the flow of power from the battery to the airframe. The ESC converts the voltage and current outputs of the battery into the input voltage and current for the motor. The motor converts the electric power from the ESC to mechanical power represented by the rotational speed and torque outputs. The propeller converts the rotational power output of the

978-1-6654-9032-0/23/$31.00 ©2023 IEEE

motor into the thrust and speed of the aircraft.

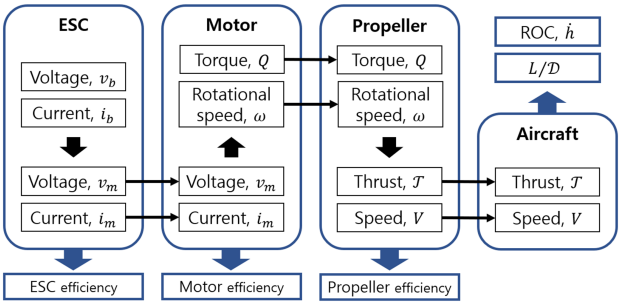

Figure 1. Power flow of the electric propulsion system.

This study presents a method that enables the optimization of the system's performance during the design process by consecutively plotting a performance map that shows the efficiency of each component. In this process, the rotational speed, ω, and torque, Q, the two variables that link the motor and the propeller, are used as independent variables.

Note that the multidisciplinary nature of this work requires the combination of notations from different disciplines that sometimes have different conventions. The standard unit for the rotational speed is "rad/s". However, because "rpm" is the most commonly used unit, all the plots are expressed in "rpm". For the analysis of the propeller, the number of rotations per second, denoted by n, is commonly used and is necessary to utilize the measurement data. This notation appears in the subsection explaining the propeller efficiencies.

ESC

As the ESCs that are used for brushless DC motors rely on fast switching of MOSFET transistors, their exist power losses due to resistance and switching. In typical efficiency models of ESCs, the efficiency is given as a function of the input voltage and current as shown in Fig. 2.

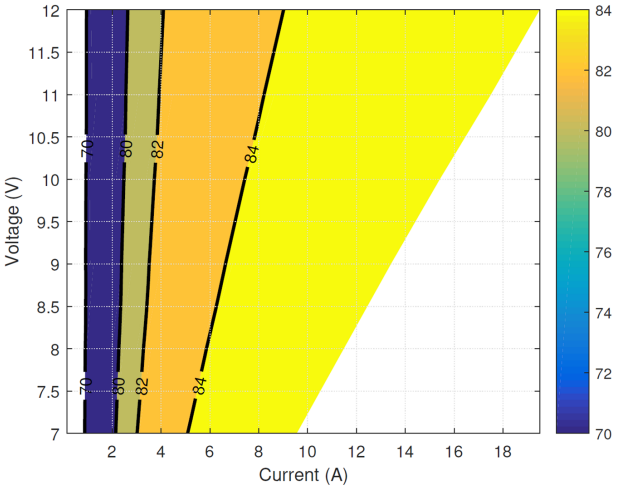

Figure 2. ESC efficiency contours of the "SuperBrain40" ESC in the v_b-i_b plane.

If v_b and i_b, respectively, represent the input voltage and current of the ESC, the ESC efficiency, η_e, is defined as in Eq. (1), where v_m and i_m denote the motor input voltage and current, respectively.

$$\eta_e = \eta_e(v_b, i_b) = \frac{v_m i_m}{v_b i_b} \tag{1}$$

Here, η_e needs to be converted to a function of Q and ω. Note that Q is the output torque of the motor, which is slightly smaller than the electromagnetic torque generated inside the motor due to friction and other losses. The input power, $v_m i_m$, is the sum of the output power, $Q\omega$, and power loss, P_L, of the motor, as expressed by Eq. (2). P_L is a function of Q and ω and is discussed in detail in the next subsection. Note that P_L is a characteristic of a specific motor.

$$v_m i_m = Q\omega + P_L \tag{2}$$

Equation (3) can be solved for i_b as a function of Q and ω for a given v_b as in Eq. (4).

$$Q\omega + P_L\left(Q, \omega\right) = v_b i_b \eta_e\left(v_b, i_b\right) \tag{3}$$

$$i_b = i_b\left(Q, \omega\right) \tag{4}$$

Finally, η_e, can be expressed as a function of Q and ω as in Eq. (5), and this process is summarized in Fig. 3.

$$\eta_e = \eta_e\left(Q, \omega\right) = \frac{Q\omega + P_L\left(Q, \omega\right)}{v_b \cdot i_b\left(Q, \omega\right)} \tag{5}$$

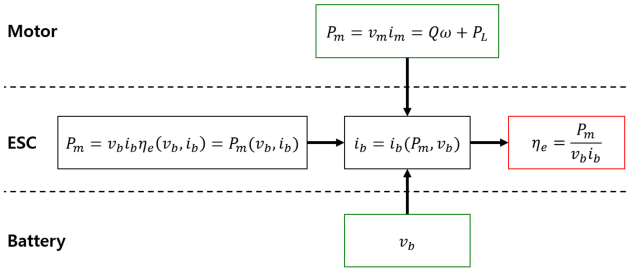

Figure 3. Information flow to calculation the ESC efficiency.

The ESC efficiency model expressed as in Eq. (6) in [2] is presented as an example.

$$\eta_e(v_b, i_b) = a_0 \frac{i_b^2}{v_b} + a_1 + a_2 \frac{1}{i_b} + a_3 \frac{1}{v_b} \tag{6}$$

where a_0, a_1, a_2, and a_3 are constants determined according to the type of ESC.

Once Eq. (6) is plugged into Eq. (3), Eq. (3) is rearranged into a cubic equation in i_b as in Eq. (7). By solving Eq. (7), i_b as a function of Q and ω as in Eq. (4) can be found.

$$a_0 {i_b}^3 + \left(a_1 v_b + a_3\right) i_b + \left(a_2 v_b - Q\omega - P_L\left(Q, \omega\right)\right) = 0 \tag{7}$$

Figure 2 shows the actual measured efficiencies of the "SuperBrain40" ESC as a function of v_b and i_b from [2]. Using

the "AT2312-1150KV" motor and assuming a battery voltage of 11.1 V, the efficiency contours of Fig. 2 are regenerated in the $\omega - Q$ plane, as shown in Fig. 4. The efficiency exceeds 80% in most areas on the map, and it increases as the motor power becomes larger. However, the peak efficiency value of 84% is relatively small, which suggests that ESC efficiency cannot be neglected, particularly when using consumer grade components.

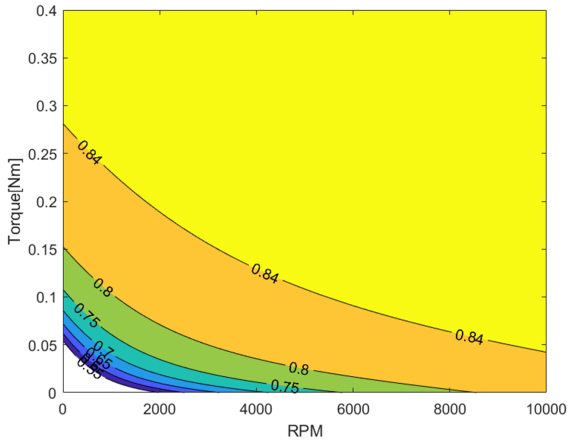

Figure 4. ESC efficiency contours of the "SuperBrain40" ESC with the "AT2312-1150KV" motor in the $\omega - Q$ plane.

Motor

The contours expressing the motor efficiency on the $\omega - Q$ plane have been widely used [4]. Previously, a simple equivalent circuit model [8], which assumes a constant friction torque for the sake of explaining the efficiency maps, was used. Figure 5 shows the efficiency contours of the "AT2312-1150KV" motor using this model. As the value of the friction torque is not provided by the manufacturer, the no load current, i_0, times the torque constant, K_t, is used for the constant friction torque. It is assumed that K_t is equal to the back-emf constant, K_e, which is provided by the manufacturer.

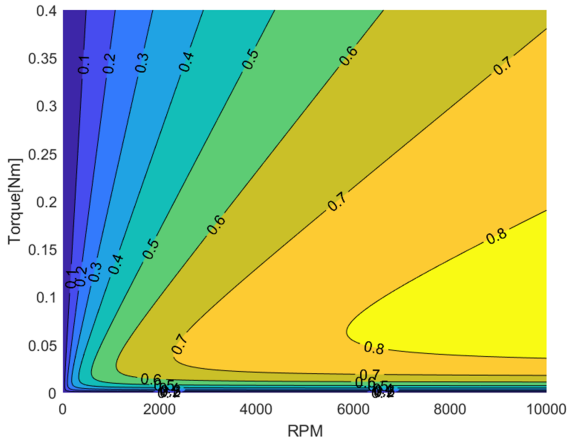

Figure 5. Efficiency contours of the AT2312-1150KV motor using the equivalent circuit model.

The loss build-up model described in [3] considers the default power loss, iron loss, and windage loss in addition to the copper and friction losses that are included in the equivalent circuit model. The power loss is expressed as in Eq. (8). The positive polynomial loss model proposed in [4] provides a way to estimate the coefficients of Eq. (8) using information that is commonly published by motor manufacturers. Once the power loss is determined, the motor efficiency is calculated using Eq. (9). This process is summarized in Fig. 6.

$$P_L(Q, \omega) = b_0 + b_1\omega + b_2\omega^3 + b_3Q^2 \tag{8}$$

$$\eta_m = \frac{Q\omega}{Q\omega + P_L} \tag{9}$$

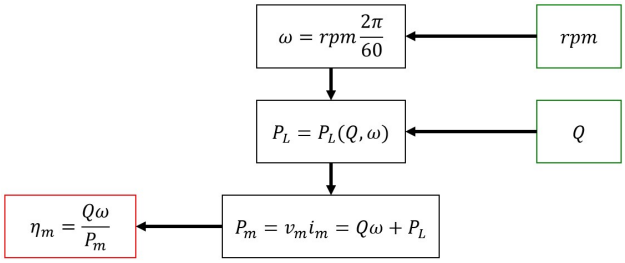

Figure 6. Information flow to calculate the motor efficiency.

Regardless of the motor model, P_L as a function of Q and ω should be used as one of the inputs for the ESC model to compute the ESC efficiency contours in the $\omega - Q$ plane.

As an example, the efficiencies of the "AT2312-1150KV" motor using the positive polynomial loss model are plotted in Fig. 7. The rotational speed at maximum efficiency, $\bar{\omega}$, maximum efficiency, $\bar{\eta}$, and the torque, $\bar{Q}$, at this rotational speed are provided by the manufacturer. The constant component in Eq. (8), b_0, means a power loss even when Q and ω are zero. Equation (10) is used to compute b_0.

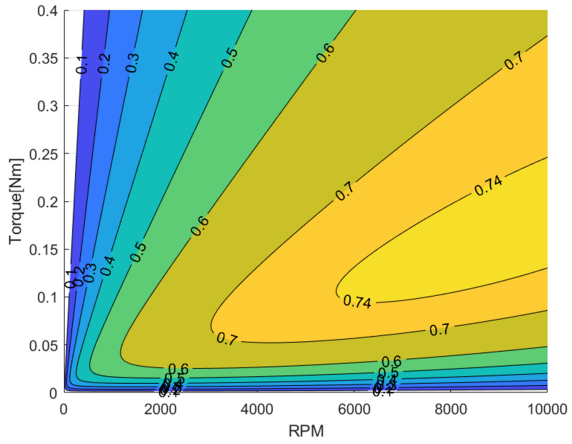

Figure 7. Efficiency contours of the AT2312-1150KV motor using the positive polynomial loss model.

$$b_0 = {i_0}^2 r \tag{10}$$

The other coefficients in Eq. (8), b_1, b_2, and b_3 are computed by solving Eq. (11) given in [4]. This relation is derived by

applying the following conditions: the derivatives $\frac{\partial P_L}{\partial Q}$ and $\frac{\partial P_L}{\partial \omega}$ are zero when the motor is operating at its maximum efficiency.

$$\begin{bmatrix} \bar{\omega} & \bar{\omega}^3 & \bar{Q}^2 \\ 0 & -2\bar{\omega}^3 & \bar{Q}^2 \\ \bar{\omega} & -\bar{\omega}^3 & 0 \end{bmatrix} \begin{bmatrix} b_1 \\ b_2 \\ b_3 \end{bmatrix} = \begin{bmatrix} -b_0 + \bar{\omega}\bar{Q}\frac{1-\bar{\eta}}{\bar{\eta}} \\ -b_0 \\ -2b_0 \end{bmatrix} \tag{11}$$

Propeller

In the previous study [8], the thrust coefficient, C_T, and power coefficient, C_P, of the propeller were assumed to be dependent only on the advance ratio, J. However, these coefficients depend on the rotational speed itself due to the Reynolds number effects. In this paper, more accurate propeller efficiency contours are presented that consider the rotational speeds. The extension is relatively straightforward because the rotational speed is already provided in every data point in the $\omega - Q$ plane, and the measurement data that corresponds to the rotational speed can be inferred. The process of finding the propeller efficiency, η_p, shown in Fig. 8 is identical to the one presented in [8], except that bilinear interpolation is used in terms of ω and J when finding J that corresponds to given Q and ω.

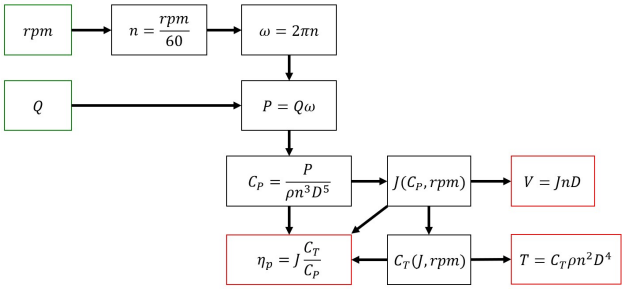

Figure 8. Information flow to calculate the propeller efficiency.

Once the J is identified, C_T that corresponds to this J and ω is obtained from the measurement data. The η_p, thrust, $\mathcal{T}$, and forward speed, V are calculated using Eqs. (12), (13), and (14), where ρ and D are the air density and the propeller diameter, respectively.

$$\eta_p = J\frac{C_T}{C_P} \tag{12}$$

$$\mathcal{T} = C_T \rho n^2 D^4 \tag{13}$$

$$V = JnD \tag{14}$$

Figure 9, 10, and 11 compare η_p, $\mathcal{T}$, and V of the "APC sport 11x7" propeller. The dotted lines represent the contours obtained using the measurement data at a single ω, 6000 rpm, whereas the solid lines show the contours obtained by using the corresponding data provided by [9].

As can be expected, the performance degradation is more noticeable at smaller rotational speeds because the data for 6000 rpm have the largest Reynolds number in the data set. Especially, the area where the propeller achieves its peak efficiency is significantly reduced. The forward speed contours are shifted slightly to the right, which means that the resulting forward speed at the same Q and ω is slightly smaller when the Reynolds number effects are considered. However, the thrust contours do not differ significantly.

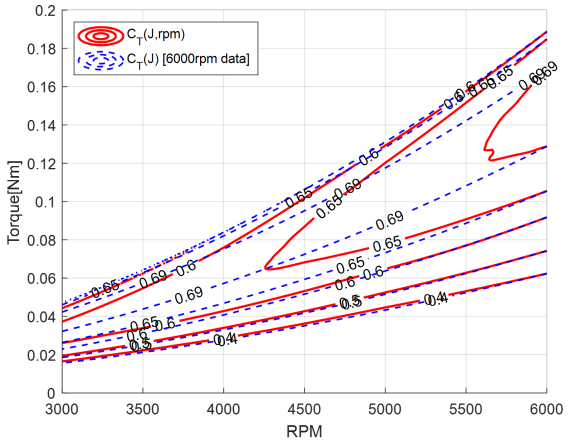

Figure 9. Comparison of the propeller efficiencies.

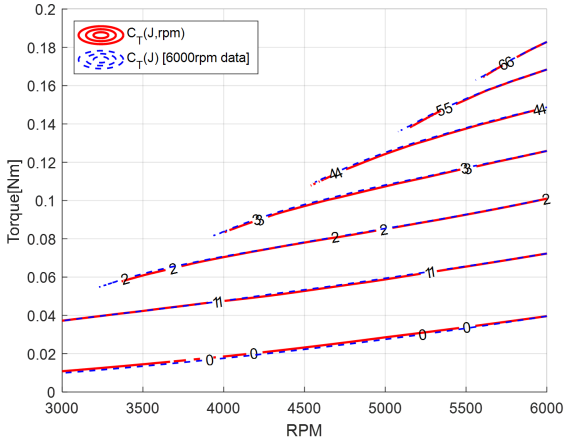

Figure 10. Comparison of the propeller thrusts.

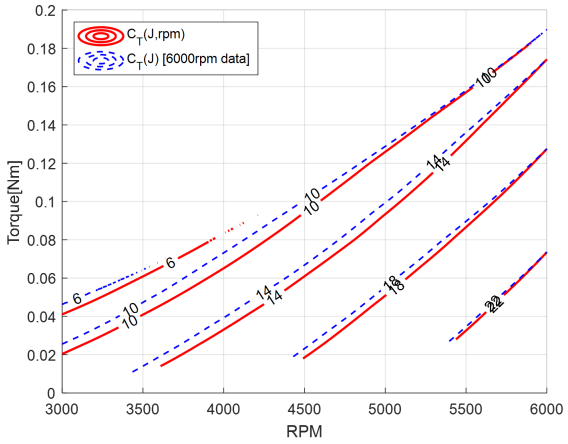

Figure 11. Comparison of the forward speeds.

Figure 12 shows the efficiency, thrust, and forward speed

contours of the "APC sport 11x7" propeller plotted together in the $\omega - Q$ plane as an example of the performance of this propeller. The propeller efficiency peaks at around 69%, as represented by the narrow yellow region that extends from the bottom left to top right. For example, at the data point at which the contours $\mathcal{T} = 6$ N and $V = 20$ m/s intersect, the rotational speed is around 7300 rpm and the torque is around 0.22 Nm. As mentioned in [8], the forward speed and thrust become the link to the final element of the system, the airframe.

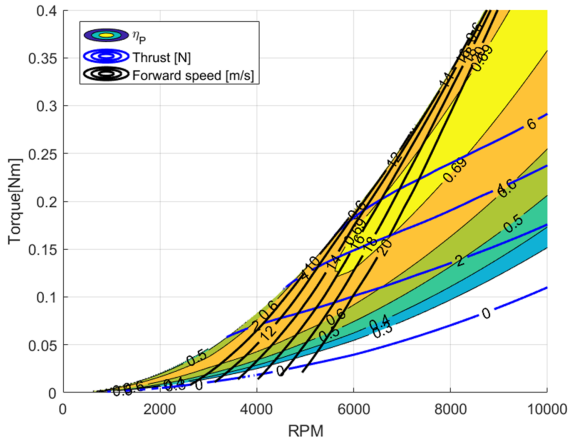

Figure 12. Efficiency, forward speed, and thrust contours of the APC sport 11x7 propeller.

Airframe

The most important data are those of the drag model of the given aircraft. The drag model can usually be approximated by the relation shown in Eq. (15). However, a more sophisticated model or measurement data could also be used. In Eq. (15), C_D is the total drag coefficient, C_{D_P} is the parasite drag coefficient, k is the overall induced drag factor, and $C_{L_{min}}$ is the lift coefficient at which the drag is minimized. Note that k should include the contribution of the lift dependent viscous drag in addition to the induced drag.

$$C_D = C_{D_P} + k(C_L - C_{L_{min}})^2 \tag{15}$$

For the airframe, the contours of the constant climb rate, $\dot{h}$, are plotted. These contours are calculated using Eq. (16), where $\mathcal{D}$ and W are the drag and weight, respectively. The process of calculating the climb rate from the speed and thrust obtained from the propeller model is summarized in Fig. 13. Calculating the climb rate instead of attempting to match the thrust and drag was one of the key enablers of this method [8].

$$\dot{h} = V\frac{\mathcal{T} - \mathcal{D}}{W} \tag{16}$$

Figure 14 shows an example of climb rate contours. When $\dot{h}$ is zero, it indicates level flight where the thrust is equal to the drag. A positive climb rate indicates the aircraft is in a steady state climb while a negative climb rate indicates the aircraft is descending.

In addition to the climb rate, other important performance parameters can be calculated. The flight power, P, defined by Eq. (17), represents the final power output of the propeller

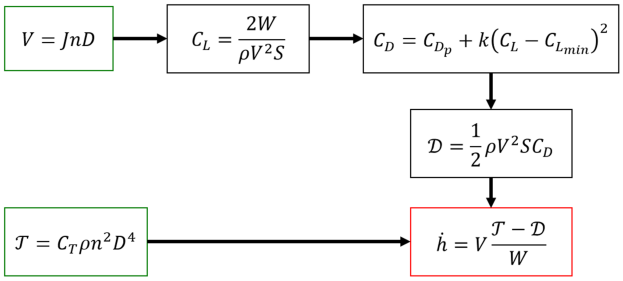

Figure 13. Information flow to calculate the climb rate.

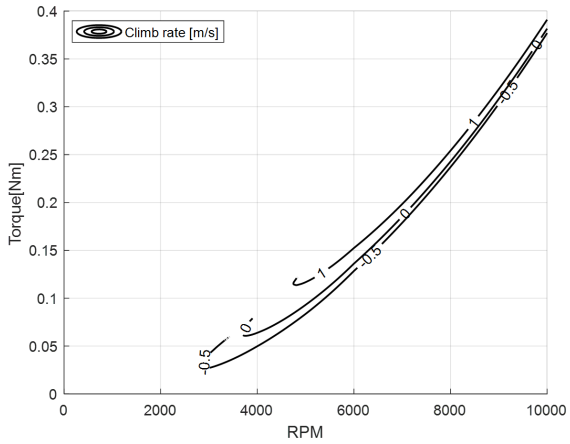

Figure 14. Climb rate contours.

to the surrounding air that provides the thrust, where S is the reference wing area of the aircraft.

$$P = \mathcal{D}V = \left(\frac{1}{2}\rho V^2 S C_D\right) V \tag{17}$$

Power consumption at the battery is larger than P because of the power losses at the propeller, motor, and ESC. If E_{batt} denotes the usable energy stored in the battery, the endurance, t_E, is calculated using Eq. (18). The range, d_R, is simply the speed multiplied by the endurance as shown in Eq. (19).

$$t_E = \eta_e \eta_m \eta_p \frac{E_{batt}}{P} \tag{18}$$

$$d_R = V t_E \tag{19}$$

3. Use Case

In this section, the methods proposed in the previous section are applied to solve the problem of finding suitable electric propulsion components for a given two meter wingspan blended-wing-body style unmanned aircraft.

Components

Two types of ESCs, motors, and propellers that form a total of eight combinations are evaluated. Two ESC models, "SuperBrain40" and "Aerostar 30A" from [2] are selected as, according to their power rating, they can accommodate

the power required for this aircraft with a certain margin. The parameters for the ESC efficiency models are listed in Table 1.

Table 1. Coefficients of the ESC efficiency model

Parameter	SuperBrain40	Aerostar 30A
a_0	0.00007030	0.00008198
a_1	0.8379	0.8019
a_2	-0.1473	-0.1767
a_3	0.2156	0.4562

The two motors "AT2312-1150KV" and "AT2820-880KV", both manufactured by T-Motor, were chosen for the analysis. The coefficients of Eq. (8) for each motor are calculated using Eqs. (10) and (11) using the measurement data provided by [10], as presented in Table 2.

Table 2. Parameters of the two motors

Parameter	AT2312 1150KV	AT2820 880KV
i_0, A	0.85	1.60
r, mΩ	75	39
$\bar{\eta}$, %	75	80
$\bar{\omega}$, rad/s	938	912
$\bar{Q}, Nm$	0.160	0.348

The two propellers, "APC sport 11x7" and "APC sport 10x8", were selected. Figures 15 and 16 show the C_T and C_P curves for four different values of the rotational speed in rpm, based on the measurement data of each propeller given in [9].

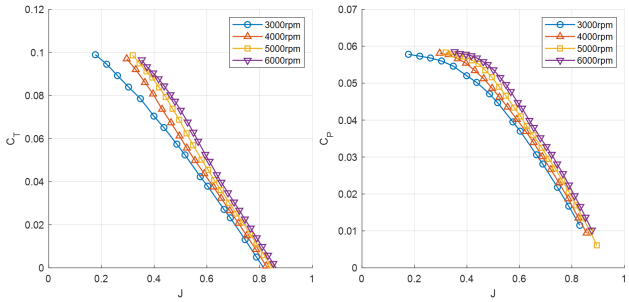

Figure 15. C_T and C_P data of the "APC sport 11x7" propeller.

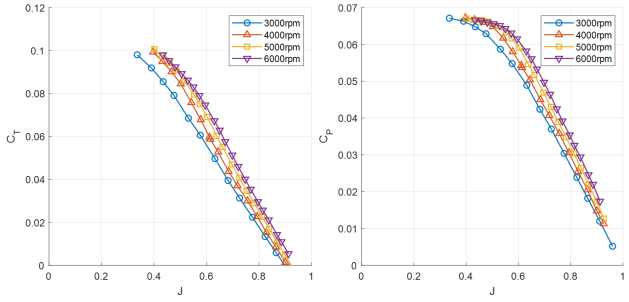

Figure 16. C_T and C_P data of the "APC sport 10x8" propeller.

The airframe to which the proposed technique was applied is shown in Fig. 17. The pusher propeller configuration at the rear end ensures minimum interference between the propeller wake and the airframe, which is advantageous for applying the proposed methodology. The specifications of the aircraft are shown in Table 3.

Figure 17. Airframe.

Table 3. Airframe parameters

Parameter	Value
Wing area, m^2	0.59
Mass, kg	2
C_{D_P}	0.0319
k	0.0974
$C_{L_{min}}$	0.1622

In this study, the characteristics of the battery were not modeled. As the internal bay of the aircraft is designed for a three-cell lithium polymer battery with a capacity of 4,000 mA, the battery is assumed to provide a fixed amount of energy. The specifications of the battery are listed in Table 4.

Table 4. Battery specifications

Parameter	Value
Voltage, V	11.1
Capacity, mAh	4,000
Energy, J	160,000

Results

The objective of the use case analysis was to determine the combination of components that maximizes the range. Table 5 lists all eight combinations of the ESCs, motors, and propellers.

Table 5. Component combinations for each case

Case	ESC	Motor	Propeller
1	SuperBrain40	AT2312	APC sport 11X7
2		1150KV	APC sport 10X8
3		AT2820	APC sport 11X7
4		880KV	APC sport 10X8
5	Aerostar 30A	AT2312	APC sport 11X7
6		1150KV	APC sport 10X8
7		AT2820	APC sport 11X7
8		880KV	APC sport 10X8

Table 6. Performance parameters for maximum level flight range

Case	ω, rpm	Q, Nm	$\mathcal{T}$, N	V, m/s	C_L	L/D	d_R, m	η_e, %	η_m, %	η_p, %	η, %
1	4,150	0.067	1.72	10.88	0.46	11.39	35,807	82.42	71.79	64.31	38.05
2	4,210	0.058	1.68	10.37	0.51	11.68	38,244	82.02	70.92	68.08	39.60
3	4,150	0.067	1.72	10.88	0.46	11.39	34,451	82.55	68.98	64.31	36.61
4	4,210	0.058	1.68	10.37	0.51	11.68	35,879	82.25	66.35	68.08	37.15
5	4,150	0.067	1.72	10.88	0.46	11.39	34,940	80.43	71.79	64.31	37.13
6	4,210	0.058	1.68	10.37	0.51	11.68	37,283	79.96	70.92	68.08	38.61
7	4,150	0.067	1.72	10.88	0.46	11.39	33,626	80.57	68.96	64.31	35.73
8	4,210	0.058	1.68	10.37	0.51	11.68	34,996	80.23	66.35	68.08	36.24

Figure 18 shows the total efficiency, climb rate, and range contours on the $\omega - Q$ map for the Case 2 combination in Table 5. The total efficiency is defined in Eq. (20) as the product of the efficiencies of the ESC, motor, and propeller.

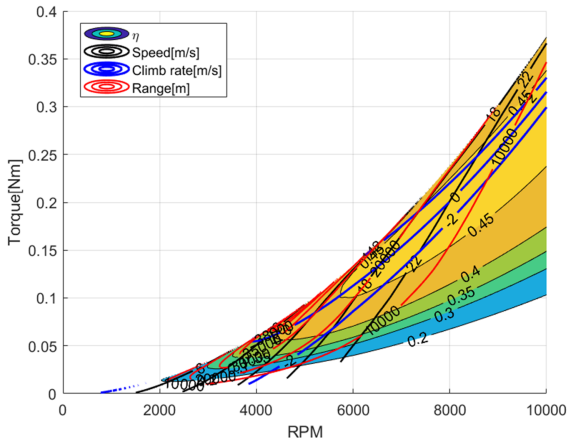

Figure 18. Total efficiency contours(Case2).

$$\eta = \eta_e \eta_m \eta_p \tag{20}$$

Figure 19 shows an enlarged view of Fig. 18 to show the point with the maximum level flight range for this combination. Note that once this point is identified, all the other performance parameters including the thrust, flight speed, lift coefficient, as well as the individual ESC, motor, and propeller efficiencies can be determined.

Table 6 lists the operational points that achieve the maximum level flight range for all eight cases. Case 2 achieved the largest range of about 38.2 km with a system efficiency of 39.6%. Case 7 resulted in the smallest range of 33.6 km with the smallest system efficiency of 35.7%. It can be observed that the range difference of 4.6 km is about 12%, which could be significant depending on the mission of the aircraft. In addition, with consumer grade components, it can be seen that around 40% is practically the maximum total system efficiency that could be achieved.

4. CONCLUSIONS

This paper presents a methodology that enables a holistic analysis of an electric propulsion system, starting from the efficiency of each component and ending with the total system efficiency under a wide range of operating conditions. In addition, each example demonstrates how to utilize commonly available data to obtain efficiency maps. If more accurate measurement data are available, they can be used to achieve more accurate system efficiency models.

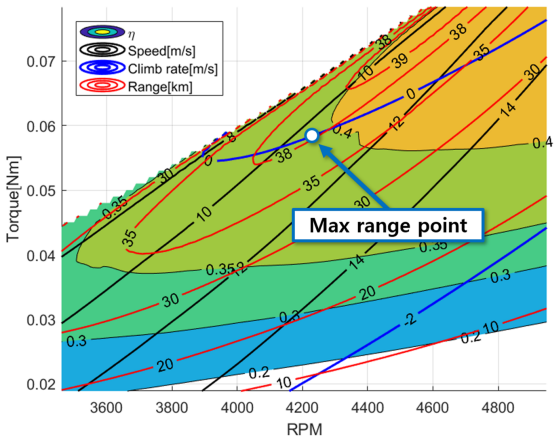

Figure 19. Maximum range point of total efficiency contours(Case2).

The methodology can be used either during the aircraft design stage or to select an optimal motor and propeller for an existing aircraft. The latter of the two, presented in this paper as a use case, demonstrates that the range can vary by more than 10% even with similar electric propulsion components.

As the methodology provides all the necessary performance information under different flight speeds and climb rates, it is expected to be useful for mission analysis or mission profile optimization as well.

ACKNOWLEDGMENTS

This work is supported by a Korea Agency for Infrastructure Technology Advancement (KAIA) grant funded by the Ministry of Land, Infrastructure and Transport(Grant 22BDASC158275-03) and a Korea Evaluation Institute of Industrial Technology grant funded by the Ministry of Trade, Industry and Energy(Grant 20016489).

REFERENCES

[1] C. Hwang, "Status and challenges of urban air mobility development," *Current Industrial and Technological Trends in Aerospace*, vol. 16, no. 1, pp. 33–41, 2018.

[2] A. Gong and D. Verstraete, "Experimental testing of electronic speed controllers for uavs," in *53rd AIAA/SAE/ASEE Joint Propulsion Conference*. [Online]. Available: https://arc.aiaa.org/doi/abs/10.2514/6.2017-4955

[3] J. Larminie and J. Lowry, in *ELECTRIC VEHICLE TECHNOLOGY EXPLAINED*, 2012, pp. 153–155.

[4] R. A. McDonald, "Electric motor modeling for conceptual aircraft design," in *51st AIAA Aerospace Sciences Meeting including the New Horizons Forum and Aerospace Exposition*, 2013.

[5] ——, "Modeling of electric motor driven propellers for conceptual aircraft design," in *53rd AIAA Aerospace Sciences Meeting*, 2015. [Online]. Available: https://arc.aiaa.org/doi/abs/10.2514/6.2015-1676

[6] A. Gong, R. MacNeill, and D. Verstraete, "Performance testing and modeling of a brushless dc motor, electronic speed controller and propeller for a small uav application," in *2018 Joint Propulsion Conference*. [Online]. Available: https://arc.aiaa.org/doi/abs/10.2514/6.2018-4584

[7] D. Duan, Z. Wang, Q. Wang, and J. Li, "Research on integrated optimization design method of high-efficiency motor propeller system for uavs with multi-states," *IEEE Access*, vol. 8, pp. 165 432–165 443, 2020.

[8] H.-T. Lee, "A technique for matching propeller, motor, and airframe of an electric powered aircraft based on efficiency maps," in *AIAA SCITECH 2022 Forum*. [Online]. Available: https://arc.aiaa.org/doi/abs/10.2514/6.2022-0885

[9] J. B. Brandt, R. W. Deters, G. K. Ananda, O. D. Dantsker, and M. S. Selig, "Uiuc propeller database," 2020. [Online]. Available: https://m-selig.ae.illinois.edu/props/propDB.html

[10] T-MOTOR Web site: store.tmotor.com.

BIOGRAPHY

Hong-Su Nam *received his B.S. degree in Aerospace Engineering from Inha University, Incheon, Republic of Korea, in 2021. He is currently a M.S. student in Aerospace Control & Systems Laboratory, Department of Aerospace Engineering, at Inha University. His research interests include air traffic management and aircraft design optimization.*

Hyeon-Su Hwang *is currently enrolled in the B.S. program at the Department of Aerospace Engineering, Inha University. Starting from 2021, he has been participating in an undergraduate internship program at the Aerospace Control & System Laboratory. He has been working on airport data including node-link models and motor-propeller performance measurements.*

Seok-Hwan Lee *is currently enrolled in the B.S. program at the Department of Aerospace Engineering, Inha University. Starting from 2022, he has been participating in an undergraduate internship program at the Aerospace Control & System Laboratory. He has been working on small unmanned aircraft aerodynamic analysis and motor-propeller performance measurements.*

Hak-Tae Lee *received his M.S. and Ph.D. degrees in Aeronautics and Astronautics from Stanford University in 2006. He is currently a professor of Aerospace Engineering Department at Inha University. Prof. Lee's research interests include air traffic management, aviation data analysis, and aircraft design optimization.*